CetZ1-dependent assembly and positioning of the motility machinery in *haloarchaea*

Hannah J. Brown[1], Md Imtiazul Islam[2], Juanfang Ruan[2,3], Matthew A. B. Baker[2], Solenne Ithurbide[1,4], Iain G. Duggin[1#]

[1]Australian Institute for Microbiology and Infection (AIMI), University of Technology Sydney, Ultimo NSW 2007, Australia

[2]School of Biotechnology and Biomolecular Sciences (BABS), University of New South Wales, Kensington NSW 2052, Australia

[3]Electron Microscope Unit, Mark Wainwright Analytical Centre, UNSW Sydney, Kensington NSW 2052, Australia

[4]Present address: Département de Microbiologie, Infectiologie et Immunologie, Université de Montréal, Montréal, QC, Canada.

[#]Correspondence: Iain.Duggin@uts.edu.au

Abstract

The tubulin-like CetZ proteins are archaeal cytoskeletal proteins that contribute to cell shape and swimming motility in the halophilic archaeon *Haloferax volcanii*. Currently it is unknown whether CetZs contribute to motility solely through their control of cell shape or in other ways too. Here, we used cryo-electron and fluorescence microscopy to observe *H. volcanii* cell surface filaments and the localisation of the motility machinery, respectively, in strains with *cetZ1* or *cetZ2* deletion, overexpression, and polymerisation-defective mutant backgrounds. Our results show that CetZ1 has an important role at the poles of mature motile rod cells for the assembly of key motility proteins, including ArlD1, a constituent of the archaellum base, and the chemotaxis sensory array adapter CheW1 and signal transducer CheY. Importantly, overproduction of CetZ1 and CetZ1-mTurquoise2 inhibited motility and reduced the frequency of localisation of the motility machinery markers but did not affect rod-shape in swimming cells. Our data suggest that CetZ1 acts as a polar cytoskeletal structure that orchestrates the assembly and positioning of both major components of the motility machinery. The multifunctionality and dynamic redeployment of CetZ1 during motile cell development is reminiscent of eukaryotic cytoskeletal proteins and the roles of tubulin at the base of the eukaryotic flagellum.

Significance statement

This study demonstrates that archaeal CetZ tubulin-like cytoskeletal proteins control swimming motility through promoting the assembly of motility structures at cell poles, in addition to their established roles in rod morphology development. To achieve this, the conserved CetZ1 protein assembles as a cap or patch-like structures at the cell poles of mature motile rod cells of the model archaeal organism, *H. volcanii*. CetZ1 migration to the cell poles for assembly of motility structures has a primitive resemblance to the roles of tubulin in basal bodies essential to the development of eukaryotic flagella. Our findings represent the discovery of both multifunctionality and dynamic redeployment in an archaeal cytoskeletal protein, combined behaviours thought to be a characteristic of the eukaryotic cytoskeleton.

Introduction

Cytoskeletal proteins are utilised as platforms or scaffolds for large protein complexes across the tree of life. Tubulin superfamily proteins are particularly widespread across all three domains, including tubulin in Eukarya, FtsZ in Bacteria and Archaea, and the Archaea-specific CetZ family[1-5]. In eukaryotes tubulin forms microtubules, which act as platforms in several different biological contexts, including for the anchoring and partitioning of chromosomes during cell division[6], intracellular transport of cargo[7, 8] and assembly of protein complexes[9] and surface appendages[10]. In bacteria, FtsZ forms a ring at mid-cell which is an essential platform required for the assembly of the divisome complex, consisting of more than thirty proteins[11]. In comparison to tubulin and FtsZ, CetZs are understudied in terms of their basic biological functions and their capacity to act as platforms or scaffolds for assembly of other protein complexes.

In the motile and pleomorphic model halophilic archaeon, *Haloferax volcanii*, CetZs have been shown to control cell shape changes and have also been implicated in swimming motility[12, 13]. *H. volcanii* has six CetZ paralogues, with CetZ1 and CetZ2 being the most highly conserved CetZs, and the only CetZs which have been functionally investigated. CetZ1 has a necessary role in rod-development, a morphological change which occurs in several conditions, including trace element depletion[14], in early log phase growth, and when cells are motile[12, 14]. Deletion of *cetZ1* and mutation of its GTPase active site, which is critical for CetZ1 polymerisation, both result in inhibition of rod-development[12, 13]. Importantly, deletion and mutation of *cetZ1* also causes a severe motility defect[12]. While deletion of *cetZ2* has not yet shown to result in any shape or motility phenotype[12], mutation of its GTPase active site prevents rod formation and causes a motility defect in a dominant inhibitory manner[12]. In addition to these observed motility phenotypes in *H. volcanii*, a survey of CetZs, motility, and rod shape across Haloarchaea found that the presence of both CetZ1 and CetZ2 in Haloarchaea species is highly correlated with motility and rod-shape[15]. With our current knowledge, the role of CetZs in motility is seemingly connected to their dominant function in cell shape control. It is not yet clear whether CetZs only contribute to motility through their control of rod-development, or whether they also participate in other mechanisms to promote swimming motility.

Previous studies have shown that CetZ1 localises strongly at poles of rod-shaped cells, either as small bright foci or as larger caps, and appeared especially bright and stable at the poles of motile rods sampled from soft agar[12, 13, 16]. As CetZs are hypothesised to be multifunctional[15], one possibility is that they may contribute to the assembly or positioning of motility protein complexes, such as the archaellum or chemosensory arrays, at cell poles. Like in bacteria, archaeal chemotaxis arrays are responsible for sensing extracellular signals and activating a signal cascade that results in a change in rotational direction of the archaellum[17-19], the whip-like structure equivalent to the

bacterial flagellum (reviewed in [20-24]). On a molecular level, chemotaxis proteins in Haloarchaea are like the bacterial system, with methyl-accepting chemotaxis proteins (MCPs), CheW, and CheA organised as a chemosensory array at the cell envelope. When extracellular signals bind to the MCPs they induce a signal cascade that results in autophosphorylation of CheA, which in turn phosphorylates CheY[18]. Phosphorylated CheY shuttles between chemosensory arrays and the archaellum base (composed of ArlD and ArlCE) where it binds and phosphorylates CheF[17, 19]. Together, ArlD and ArlCE are responsible for signal transduction to the archaellum motor proteins (ArlH, ArlI, ArlJ) and highly depend on these motor proteins for localisation at the cell poles[18]. ArlD and ArlCE are thought to directly bind the archaellum motor[25, 26] but are also presumed to bind a hypothesized polar cap or cytoplasmic cone structure at the cell poles[18].

Polar caps are large cytoplasmic structures which are situated adjacent to the inner membrane in motile euryarchaea. They have been identified in *Pyrococcus furiosus*[26], *Thermococcus kodakarensis*[25], and *Halobacterium salinarum*[27]. In all cases, the polar caps have been found to act as polar organising centres associated with archaella bundles. In *P. furiosus* and *T. kodakarensis*, polar caps were also associated with chemosensory arrays. A polar cap has not yet been identified in *H. volcanii*, and the proteins which compose polar caps in euryarchaea are not yet known.

We hypothesized that CetZs, typical of scaffold forming cytoskeletal proteins, may be able to act as a platform or polar cap-like structure in *H. volcanii*, and contribute to motility via mechanisms independent from their control of cell shape. Hence, in this study we investigated the potential for CetZs to contribute to motility via assembly and positioning of archaellum and chemotaxis structures. The results are consistent with a key role for CetZ1 in the assembly and positioning of motility protein complexes at the poles of motile cells, and our study thus provides the first indication that CetZs have structural and organisational roles for the assembly of protein complexes at the cell surface.

Methods

Growth and genetic modification of H. volcanii

H. volcanii was routinely grown in Hv-Cab or Hv-YPCab medium[14] supplemented with 50 µg/mL uracil if necessary to fulfil auxotrophic requirements of strains, or with L-Tryptophan to induce expression of genes of interest from pTA962-based[28] expression plasmids. Cultures were grown at 42 °C with shaking (200 rpm). *H. volcanii* was transformed with demethylated plasmids extracted from *E. coli* strain C2925 using the previously described method[29].

H. volcanii H26 (ID621) was used as the wildtype background and as the parent strain of the Δ*cetZ1* (ID622) and Δ*cetZ2* (ID357) strains, which were generated as in-frame deletions of *cetZ1* (HVO_2204) or *cetZ2* (HVO_0745) using the previously described plasmids pTA131_2204_IF[16] and pTA131_CetZ2[12], respectively and 'pop-in pop-out' method[30]. For all experiments, *H. volcanii* strains contained the pTA962 shuttle vector (control strains) or vectors for expression of relevant genes. Strains are listed in Table S1.

Plasmid construction

All reagents for plasmid construction were obtained from New England Biolabs and used according to the manufacturer's instructions, and oligonucleotides were obtained from Integrated DNA Technologies. Plasmids and oligonucleotides used for cloning detailed in Tables S2 and S3, respectively. To generate a plasmid for the expression of CetZ2-EG-mTurquoise2, the *cetZ2* ORF was amplified from pTA962-CetZ2 using a reverse primer to remove the stop codon and incorporate a BamHI restriction site to the 3' end. The amplified ORF was then ligated between NdeI and BamHI in pHVID21[16].

For plasmids for dual expression of untagged CetZs and GFP tagged motility proteins, ORFs for ArlD1-GFP, GFP-CheW1, and CheY-GFP were amplified from pSVA3919, pSVA5031, and pSVA5611, respectively, incorporating a BglII restriction site at the 5' end, and a NotI site at the 3' end. After purification and restriction digestion, these ORFs were ligated between BamHI and NotI sites of pTA962-CetZ1, pTA962-CetZ2, pTA962-CetZ1.E218A, and pTA962-CetZ2.E212A, utilising the compatible ends generated by BglII and BamHI. The resulting vectors contained the p.*tna* promotor, immediately followed by the CetZ ORF and then the ArlD1, CheW1, or CheY-GFP fusion ORF which was maintained in-frame. The sequences of all constructed plasmids were confirmed by Sanger sequencing (Australian Genome Research Facility).

Soft-agar motility assays

To prepare cultures for soft-agar motility assays, single colonies were inoculated into Hv-Cab medium with 1 mM L-Tryptophan and grown to an approximate OD_{600} of 0.6 overnight.

154 Following this, cultures were passaged into fresh Hv-Cab medium with 1 mM L-
155 Tryptophan every 24 hours for three days. All cultures were normalised to the same
156 starting OD_{600} before spotting 2 µL of culture onto the soft agar.

157 Hv-Cab soft-agar containing 1 mM L-Tryptophan was prepared the day before inoculation
158 of cultures onto the agar. For experiments quantifying halo size, 0.25% agar was used,
159 and motility plates were incubated for 3 days at 42 °C. This concentration of agar resulted
160 in better uniformity of halo shape and reproducibility of halo size, which was quantified
161 by taking the mean of two perpendicular measurements of the halo diameter. Motility
162 assays prepared for subsequent microscopy of halo edge cells used 0.3% agar instead,
163 and were incubated for 4-5 days at 42 °C. This method sometimes resulted in irregularly
164 shaped motility halos but produced a more defined leading edge for easier extraction of
165 cells from the agar for analysis by microscopy.

166 ***Light microscopy***

167 Cells were extracted from the edge of motility halos by stabbing the agar with a
168 micropipette (5-10 µL) near the bottom of the agar plate. After pipetting up and down
169 several times to liquify the soft-agar and release the cells, the sample was transferred to
170 a glass slide with a pad containing 1.5% agarose and 18% Buffered Salt Water (BSW)[30]
171 before covering with a #1.5 glass coverslip. All phase-contrast and fluorescence
172 microscopy were conducted on the V3 DeltaVision Elite (GE Healthcare) with filter sets
173 for GFP/FITC (excitation=464-492 nm, emission=500-523 nm) and mTurquoise2/CFP
174 (excitation=400-453 nm, emission=463-487 nm), an 100X Olympus UPLSAPO/NA 1.4
175 objective, and pco.edge 5.5 sCMOS camera. Exposure settings were always maintained
176 between all strains expressing the same fusion protein.

177 ***Light microscopy image analysis***

178 To analyse cell shape characteristics and analysis of fluorescence and localisation of
179 fluorescent fusion proteins within cells, MicrobeJ v5.13I[31] was used, a plugin for FIJI
180 v2.14.0/1.54f[32]. Unless otherwise mentioned, all settings in MicrobeJ were left as
181 default. Phase-contrast images were used to detect cell outlines using the default
182 thresholding algorithm and a cell area restriction of 1.0-max μm^2. Fluorescent
183 localisation was analysed using the *foci* detection method, restricting foci area to 0.01-
184 0.75 μm^2. Due to large variance in focus intensity and background fluorescence between
185 genetic backgrounds and plasmids, the tolerance and Z-score parameters had to be
186 adjusted for each strain as needed for accurate foci detection, but foci detection
187 parameters were maintained between biological replicates. Heatmaps of foci
188 localisation were generated using the *XYCellDensity* function, and all other image
189 analysis outputs were extracted from the MicrobeJ results tables.

190 A FIJI macro and python scripts were written and used to conduct local cell curvature
191 analysis and correlation with fluorescence intensity, based on a previously used
192 approach[12]. In short, local curvature was analysed using phase-contrast images and
193 the Contour Curvature v1.1.x (www.gluender.de) plugin in FIJI with the number of contour
194 samples set to 100, and number of coefficient pairs set to 10. The local curvature at each
195 contour sample was recorded, and these values were used to calculate the relative
196 standard deviation of curvature for each cell. The mean fluorescence intensity along the
197 cell outline generated by Contour Curvature was measured using a 3-pixel line width and
198 was correlated with local curvature by calculating the Pearson Correlation Coefficient
199 between fluorescence intensity and local curvature for each individual cell. A summary
200 of the image acquisition and analysis pipeline for light microscopy is provided in Figure
201 S3.

202 ***Cryo-Electron Microscopy and analysis***

203 To maximize the number of cells per sample for cryo-electron microscopy, cultures were
204 grown from a theoretical starting OD_{600} of 0.0005 in Hv-YPCab[14] medium and harvested
205 at OD_{600}~0.25 (after ~24 hours). A 4.5 µL droplet of the culture was applied to glow
206 discharged copper grids (Quantifoil R2/2, Quantifoil Micro Tools) and blotted for 2.5 s in
207 a 95% humidity chamber at 20 °C. The grids were then plunged into liquid ethane using a
208 Lecia EM GP device. The grids were imaged using a Talos Arctica cryo-TEM (Thermo Fisher
209 Scientific), operating at 200 kV with the specimen held at liquid nitrogen temperature.
210 Images were captured at 17,500X magnification using a Falcon 3EC direct electron
211 detector in linear mode. The number of surface filaments per cell (Fig. 1d, e) was
212 manually counted using Cryo-TEM images. This was conducted independently and
213 blindly by three individuals.

Results

CetZ1 and CetZ2 influence motility independently of cell shape control

CetZ1 and CetZ2 have previously been implicated in the control of cell motility[12], however it is not yet clear whether they solely contribute to motility through their control of cell shape, or whether they can influence motility independently of cell shape. To begin to investigate this, we first quantitatively measured the impact of *cetZ1* and *cetZ2* deletion and overexpression on motility in soft-agar, where cells swim out from a central inoculation site forming a halo (Fig. 1a). We also assessed the shape of motile cells withdrawn from the leading edge of the halo by image analysis of cell circularity, which is inversely related to cell elongation (Fig. 1b).

Deletion of *cetZ1* caused a severe motility defect, approximately 12% of wildtype motility (Fig. 1a), and prevented rod-formation in cells extracted from the leading edge of motility halos (Fig 1b), as previously reported with a different genetic background [12]. Importantly, overexpression of *cetZ1* in the wildtype or Δ*cetZ1* background reduced motility to approximately 75% of the wildtype control (carrying the vector only), despite cells at the leading edge still forming rods to the same degree as wildtype (Fig. 1a, b).

Deletion of *cetZ2* was previously reported to have no effect on motility or rod shape[12], which was confirmed here in motile cells (Fig. 1a). However, we also discovered that overexpression of c*etZ2*, whether in wildtype or Δ*cetZ2*, resulted in a mild increase in motility, approximately 115% of wildtype (Fig. 1a). This also did not result in a clear change in cell shape (Fig. 1b).

We also investigated the interdependency of the overexpression phenotypes. Overexpression of *cetZ1* in the Δ*cetZ2* background caused reduced motility like it did in the wildtype background, indicating that the effects of *cetZ1* are independent of *cetZ2* (Fig. S1a). Overexpression of *cetZ2* in the Δ*cetZ1* background failed to rescue the Δ*cetZ1* motility defect and did not clearly stimulate motility in this strain. Lastly, overexpression of the GTPase (T7 loop) mutants (*cetZ1*.E218A and *cetZ2*.E212A) inhibited motility and rod shape in the H26 background, as previously reported in H98[12], and had consistent effects in the *cetZ1* and *cetZ2* deletion strains (Fig. S1), suggesting that GTPase activity is necessary for the overexpression phenotypes of *cetZ1* and *cetZ2*.

Importantly, the above experiments indicated that CetZs can promote motility through mechanisms independent of cell shape. This led us to hypothesise that CetZs are involved in assembly or function of other cell envelope or motility structures such as the archaellum or chemosensory arrays.

CetZ1 and CetZ2 influence the frequency of cell surface filaments

To investigate whether CetZs influence the overall appearance of surface filaments such as pili and archaella, we used cryo-EM (Fig. 1c) to compare the wildtype, *cetZ1* deletion and *cetZ2* overexpression strains, which showed the most substantial and opposing effects on motility. Deletion of *cetZ1* resulted in a significant reduction in the number of surface filaments per cell, whereas overproduction of CetZ2 resulted in slightly more (Fig. 1d), which are thus consistent with the observed motility phenotypes and potential changes in archaellum assembly.

By comparing surface filament frequency in rods and plate-shaped cells, we found that in the rod-forming wildtype and *cetZ2* overexpression strains, rod-shaped cells had significantly more surface filaments compared to plate-shaped cells (Fig. 1e), suggesting as expected that cell shape correlates with the assembly of surface filaments. Interestingly, the number of surface filaments in the Δ*cetZ1* strain was still lower than the number of surface filaments in plate-shaped wildtype cells (Fig. 1d, e). Plates can be motile as shown by timelapse imaging albeit with reduced speeds[12]. These observations suggest that the motility defect of Δ*cetZ1* is not only linked to its rod shape defect, but also a reduction in surface filaments such as the archaellum.

Functional CetZ-mTq2 fusions localise to cell poles in motile cells

CetZ1 was initially reported to localise strongly to cell poles in rod-shaped cells[12], however since the CetZ1-GFP fusion was not fully functional as a sole copy in rod-development, it remained unclear whether the polar localisation reflected a native function of CetZ1. Subsequent studies of CetZ1 localisation using an almost fully functional CetZ1-mTurquoise2 (mTq2) fusion have not investigated CetZ1 localisation in motile cells[13, 16]. Therefore, we next used the existing CetZ1-mTq2 fusion and generated a CetZ2-mTq2 fusion to observe the localisations of CetZ1 and CetZ2 in motile cells extracted from the leading edge of soft-agar motility halos.

CetZ1-mTq2 and CetZ2-mTq2 were first tested for their capacity to support motility in their respective *cetZ* knockout backgrounds (Fig. 2). CetZ1- and CetZ2-mTq2 fusions produced motility halos that were on average 71% and 107% of the size of those produced by expression of untagged *cetZ1* and *cetZ2*, respectively (Fig. 2a). These differences in motility were statistically significant between Δ*cetZ1*+CetZ1 and Δ*cetZ1*+CetZ1-mTq2, but not between Δ*cetZ2*+CetZ2 and Δ*cetZ2*+CetZ2-mTq2. Notably, neither CetZ1-mTq2 nor CetZ2-mTq2 had a substantial effect on the shape of motile rods when expressed in the wildtype or knockout backgrounds, further supporting the notion that CetZ roles in motility involve but extend beyond supporting mature rod shape of swimming cells (Fig. 2b).

In motile cells extracted from the halo edge, both proteins displayed bright patches at cell poles (Fig. 2c-e). CetZ1-mTq2 showed additional patchy localisation around the inner membrane and at mid-cell as previously described (Fig. 2c)[12, 13, 16]. These similarities

287 and differences in CetZ1-mTq2 and CetZ2-mTq2 localisations were clearly reflected in
288 heat map representations of foci localisation along normalized longitudinal and lateral
289 cell axes (Fig. 2d). No differences in localisation were observed when either CetZ-mTq2
290 fusion was expressed in the wildtype or their knockout genetic background. The polar
291 localisations of CetZ1 and CetZ2 are consistent with the hypothesis that they may
292 participate in the assembly or positioning of motility structures, like the archaellum, at
293 the cell poles.

294 ***CetZ1 influences the positioning and assembly of ArlD1***

295 Given the above results, we proceeded to use fluorescence microscopy to determine
296 whether CetZ1 and CetZ2 affect the assembly or positioning of key motility proteins.
297 These included ArlD1 as a marker for the archaellum base, CheW1 as a marker for
298 chemosensory arrays, and CheY, the effector protein which shuttles between
299 chemosensory arrays and the archaellum base. These three proteins were considered
300 good candidates to understand how the CetZs influence assembly and positioning of
301 motility proteins, as their localisations in motile cells have been well characterised[17,
302 18] and expression of ArlD1-GFP, GFP-CheW1, and CheY-GFP did not cause substantial
303 motility or cell shape defects in wildtype (Fig. S2) or *cetZ* mutant backgrounds as
304 described below. For ArlD1, CheW1, and CheY, the number of foci per cell was used to
305 assess their degree of assembly, and for rod-forming strains, the percentage of foci
306 located at cell poles was used as an indicator of correct positioning. As some mutations
307 of CetZs (*cetZ1* deletion, CetZ1.E218A, and CetZ2.E212A) result in significant inhibition
308 to rod-formation, we also measured the degree to which curvature of the cell outline
309 correlated with fluorescent signal of the motility proteins in individual cells (Fig. S3), and
310 across the population of cells.

311 In wildtype motile cells, ArlD1-GFP localised as bright foci at the cell poles (Fig. 3a, S4c),
312 with most cells having two foci (Fig. 3e), one at each pole, as has been previously
313 observed[17]. The vast majority (>97%) of detected foci were located at cell poles (Fig.
314 S4b), and across the population, membrane curvature strongly correlated with
315 fluorescence (Fig. 3f). In the Δ*cetZ1* background, ArlD1-GFP localised as discrete foci
316 adjacent to the cell edges in some cells (Fig. 3b, S4c), however most cells either had one,
317 or no foci (Fig. 3e). In addition, there was no correlation between membrane curvature
318 and ArlD1 localisation (Fig. 3f). When *cetZ1* was overexpressed, the number of ArlD1-GFP
319 foci (Fig. 3e) and their association with membrane curvature (Fig. 3f) was reduced,
320 consistent with the reduced swimming motility of this strain (Fig. 1a). Production of
321 CetZ1.E218A at relatively high levels disrupts cell shape, resulting in a heterogeneous
322 population of irregularly shaped and enlarged plate-shaped cells (Fig. 3b, S1)[12]. In the
323 larger cells, ArlD1-GFP localised as many foci distributed throughout the cell and not at
324 the cell edges (Fig. S4c), while the smaller plate-shaped cells showed low or no localised
325 fluorescent signal. Image analysis showed that across the population, the number of

326 ArlD1 foci per cell was increased in comparison to wildtype cells (Fig. 3e), and there was
327 a negative correlation between the localisation of ArlD1 and membrane curvature (Fig.
328 3f). Together these data demonstrate that CetZ1 is important for correct positioning and
329 assembly of ArlD1, but that it is not the only factor important for assembly, as ArlD1 still
330 formed discrete foci in the absence of CetZ1.

331 Deletion of *cetZ2* (Fig. 3b) had no effect on the assembly (Fig. 3e) or localisation (Fig. 3f,
332 S5b, c) of ArlD1 at cell poles, consistent with the lack of motility and cell shape
333 phenotype exhibited by this strain (Fig. 1a, b)[12]. Interestingly, overproduction of the
334 CetZ2.E212A GTPase mutant resulted in a more moderate effect than the CetZ1.E218A
335 GTPase mutant. While rod shape was inhibited, as with production of CetZ2.E212A alone
336 (Fig. S1b, c), resulting cell shapes were not highly irregular. In addition, ArlD1 localisation
337 appeared more like that described for the Δ*cetZ1* background. Foci number per cell (Fig.
338 3e) was reduced compared to the wildtype background, and correlation with membrane
339 curvature was substantially reduced (Fig. 3f). When CetZ2 was overproduced (Fig. 3b),
340 ArlD1 positioning at cell poles was not substantially affected (Fig. 3f, S5b, c). However,
341 CetZ2 overproduction counterintuitively resulted in less ArlD1 foci per cell (Fig. 3e)
342 despite our observation that this strain had increased motility (Fig. 1a) and has overall
343 more surface filaments (Fig. 1c). One possible explanation is that the increased number
344 of surface filaments is not observable by light microscopy due to clustering or
345 localisation of filaments near one another. Overall, these observations point to a
346 synthetic role of CetZ2 in motility by promoting of archaellum assembly when it is
347 overproduced; *cetZ2* deletion showed no impact on ArlD1 positioning or assembly.

348 ***CheW1 assembly is highly dependent on CetZ1***

349 Strikingly, we found that CetZ1 was had a major impact on the assembly (localisation) of
350 the chemotaxis array marker protein GFP-CheW1; deletion of *cetZ1* resulted in diffuse
351 localisation of GFP-CheW1, with only a small proportion of cells displaying 1-2 faint foci
352 (Fig. 4b, 4e) in comparison to two or more polar-localised foci in the wildtype background
353 (Fig. 4a, 4e, S6c). Fluorescence intensity of GFP-CheW1 also was not correlated with
354 membrane curvature as it is in the wildtype background, likely due to the strong reduction
355 in localisation of this protein in the absence of CetZ1 (Fig. 4f). Overproduction of CetZ1
356 reduced the number of foci per cell (Fig. 4e), and their localisation at areas of membrane
357 curvature (Fig. 4f, S6b, c), consistent with the resulting reduced motility (Fig. 1a). The
358 CetZ1.E218A GTPase mutant had a similar inhibitory effect on CheW1 localisation as it
359 did on ArlD1, substantially disrupting cell shape, CheW1 localisation (Fig. 4b, S6c), and
360 association with membrane curvature (Fig. 4f). Together these observations suggest
361 CetZ1 is a key driver of CheW1 assembly.

362 Deletion of *cetZ2* had no effect on foci number (Fig. 4e) or positioning of CheW1 (Fig. 4f).
363 Differently from the effect of CetZ2.E212A production on ArlD1 assembly, CheW1

364 localisation was diffuse (Fig. 4b), with the vast majority of cells having no discrete CheW1
365 foci (Fig. 4e), and GFP-CheW1 fluorescence showing no correlation with membrane
366 curvature (Fig. 4f, S6c). Additionally, overproduction of CetZ2 caused no difference in
367 CheW1 foci number (Fig. 4e), conversely to what was observed with ArlD1 (Fig. 3e). CetZ2
368 overproduction did however cause CheW1 to localise less strongly at the cell poles which
369 was observable by microscopy (Fig. 4b, S6b, c) and through the reduced correlation of
370 GFP-CheW1 fluorescence with membrane curvature (Fig. 4f).

371 ***CetZ1 is important for CheY assembly and positioning***

372 Following these observations of the impacts of CetZs on the assembly of archaellum and
373 chemotaxis structures, we next wanted to determine whether CetZs also influence the
374 effector protein, CheY, which shuttles between chemosensory arrays and the archaellum
375 base as part of the signal transduction pathway which results in switching of rotation
376 direction of the archaellum. Generally, we observed that the effect of *cetZ1* deletion,
377 overexpression, and GTPase mutation on CheY localisation was like that of CheW1. All
378 three mutations disrupted CheY localisation (Fig. 5b, S7c) by reducing the number of
379 CheY foci per cell (Fig. 5e), as well as the correlation of CheY positioning with regions of
380 high membrane curvature (Fig. 5f). Like with ArlD1 and CheW1, production of
381 CetZ1.E218A also produced a sub-population of large and highly irregularly shaped cells
382 with several CheY foci (Fig. 5b). This might indicate that CetZ1 is important for CheY
383 shuttling directly or through its impact on CheW1 assembly and positioning (Fig. 4).

384 Deletion of *cetZ2* also had no effect on assembly or positioning of CheY, and production
385 of CetZ2.E212A had similar effects as those on CheW1 assembly and positioning (Fig. 5b,
386 e, f, S7b, c). CheY-GFP signal was diffuse in most cells, resulting in reduced foci number
387 and correlation between CheY localisation and membrane curvature. Overproduction of
388 CetZ2 resulted in less CheY foci per cell, and like CheW1, correlation between CheY
389 localisation and membrane curvature was reduced. The percentage of detected CheY
390 foci present at cell poles when CetZ2 was overproduced was also significantly reduced
391 compared to the wildtype background (Fig. S7b).

392 **Discussion**

393 Several genes in *Haloferax volcanii* have been shown to affect motility, including genes
394 encoding archaella components and its assembly[17, 18, 33], chemotaxis[17, 19],
395 glycosylation[34, 35], lipid modification[36, 37], adhesion[38], as well as transmembrane
396 proteases[34, 39], KaiC-like ATPases[40], transcriptional regulators[41], a multitude of
397 genes with unknown functions[42-45], and cytoskeletal proteins[12, 46, 47]. CetZ
398 tubulin-like proteins in archaea have previously been implicated in the control of cell
399 shape and motility in *H. volcanii*[12], however the molecular mechanisms used by CetZs
400 to control these cellular processes have not yet been described. Rod shape, which is
401 controlled by CetZ1[12, 13], is highly correlated with motility in Haloarchaea[12, 15, 48].
402 There are a few likely contributing factors to this correlation. Rod-shape itself may
403 provide directionality and a more streamlined cell shape for swimming[49]. Additionally,
404 rod-shaped cells have a polarity which can be a cue for the correct assembly and polar
405 placement of polar motility machinery. For example, the MinD4 positioning protein
406 oscillates between and localises at the cell poles to control the positioning of ArlD1 and
407 CheW1[50]. In plate-shaped cells, which do not have such polarity, MinD4 circles instead
408 of oscillates, and while ArlD1 is still assembled and localised, the archaellum filament
409 and chemosensory arrays are not[17, 50], demonstrating the importance of rod shape
410 and polarity in the assembly mechanism of these polar motility complexes.

411 Here, we identified that although some manipulations of CetZs (Δ*cetZ1,* +CetZ1.E218A,
412 +CetZ2.E212A) exhibit both rod-shape and motility defects (also demonstrated in [12]
413 and [13]), overproduction of either CetZ1 or CetZ2 result in motility phenotypes without
414 affecting cell shape (Fig. 1a, b, S1). This shows that in addition to their role in controlling
415 cell shape, CetZs are likely to also contribute to motility through separate mechanisms.
416 Following these observations, we focused on investigating the role of CetZ1 and CetZ2 in
417 assembly and positioning of motility proteins ArlD1, CheW1, and CheY, testing the
418 hypothesis that they may contribute to motility by acting as a scaffold or platform for the
419 assembly of archaella and chemosensory array protein complexes.

420 Although overproduction of CetZ2 resulted in an increase in motility and the number of
421 surface filaments, it did not appear to promote the assembly or positioning of ArlD1,
422 CheW1, or CheY at the resolutions achievable by fluorescence microscopy. Instead,
423 overproduction of CetZ2 resulted in slightly less efficient localisation of these proteins at
424 cell poles, which may be a result of tightly clustered proteins within proximity to one
425 another. From these data alone, the mechanism behind hypermotility resultant from
426 CetZ2 overproduction is still unclear.

427 As deletion of *cetZ2* had no impact on cell shape, motility (as previously observed in [12]),
428 or assembly and positioning of ArlD1, CheW1, or CheY, we believe the motility
429 phenotypes resulting from overproduction of CetZ2 and CetZ2.E212A are likely to be
430 synthetic consequences of overproduction, and CetZ2 most likely does not have a

431 significant role in motility, at least under the conditions investigated where CetZ2 protein
432 levels are expected to be low[51]. Therefore, we believe it is likely that the level of CetZ2
433 during mid-log phase or in motile rods is too low to result in any cell shape or motility
434 phenotype when deleted. Here, and in previous work[12], the CetZ2 GTPase mutant has
435 been demonstrated to function within cell shape and motility pathways, so perhaps
436 CetZ2 has an important role in the control of cell shape or motility in other conditions
437 instead.

438 The different effects of deletion, overproduction, or GTPase mutations of CetZ1 and
439 CetZ2, in addition to their strong conservation throughout haloarchaea and their distinct
440 phylogenetic groupings, demonstrates that CetZ1 and CetZ2 are likely to have distinct
441 functions. Here we observed that CetZ1 overproduction in the absence of CetZ2 still
442 reduced motility equivalently to the wildtype background. However, CetZ2
443 overproduction did not complement the motility defect caused by deletion of *cetZ1*,
444 indicating CetZ1 and CetZ2 are not redundant proteins. As previously reported[12],
445 CetZ2.E212A dominantly blocks rod shape even though deletion of *cetZ2* has no effect
446 on the shape of motile cells, suggesting it inhibits CetZ1-mediated maturation of motile
447 rods[12]. Further work must be carried out to understand the endogenous function of
448 CetZ2.

449 CetZ1 demonstrated obvious effects on both the positioning and assembly of ArlD1,
450 CheW1, and CheY, but had a particularly strong influence on the latter two chemotaxis
451 proteins. Deletion or overexpression of *cetZ1*, as well as production of the CetZ1.E218A
452 dominant-inhibitory GTPase mutant all reduced assembly and polar positioning of ArlD1,
453 CheW1, and CheY to varying degrees, consistent with their observed motility defects. The
454 reduction in swimming motility and localisation of motility markers upon overproduction
455 of CetZ1 suggests that the excess CetZ interferes with the proper assembly of the motility
456 proteins[52].

457 We also confirmed, using functional CetZ1-mTq2 fusions, that CetZ strongly localises to
458 the poles of motile rods, which differs compared to the longitudinal filaments and
459 dynamic foci seen in rods and during rod formation in liquid culture[12, 13]. Notably, a
460 CetZ1-mTq2 fusion fully supported rod shape in swimming cells (Δ*cetZ1* background),
461 but motility was reduced compared to the untagged CetZ1. This further supports the
462 notion that these two functions of CetZ1 occur independently. Together, these
463 observations demonstrate that while CetZ1 is required for mature rod-shape of motile
464 cells, it also has a mechanistic role in the positioning and assembly of archaella and
465 chemotaxis arrays. Our findings are thus consistent with the general hypothesis that
466 CetZ1 is an upstream player in the assembly of polar protein complexes in addition to
467 aiding motility through its control of rod-shape.

468 Polar cap structures have been identified in several archaeal species, including
469 *Thermococcus kodakarensis*[25], *Pyrococcus furiosus*[26], and a relative of *H. volcanii*,

Halobacterium salinarum[53]. Although hypothesized[18], a polar cap has not been identified in *H. volcanii*, and it is not known what components constitute the cap structures in other archaea. Together with the observation that CetZ1 strongly localises at the cell poles of motile cells, our data suggests a new role of CetZ1 as a functional component of a polar cap in *H. volcanii*. CetZ1 forms protofilaments which assemble laterally into sheets and are predicted to interact with the inner membrane[12, 13]. We predict that such sheet-like structures might assemble and help form the cell poles and promote assembly of motility structures there.

Both CetZ1 and CetZ2 have even been identified as potential interacting partners with several chemotaxis proteins (including CheW1 and CheY) by affinity purification mass spectrometry in *H. salinarum*[54], which is known to have a polar cap[53], further indicating the potential for CetZs to interact with protein complexes at cell poles in *H. volcanii*. These previous findings are consistent with the strong effect of CetZ1 on chemotaxis protein positioning and assembly we observed in *H. volcanii*. High resolution structural and compositional analysis of cap structures in *H. volcanii* will be valuable towards determining the exact structural role of CetZ1 at cell poles. With CetZ1 and MinD4[50] both implicated in the positioning of archaella and chemosensory arrays at cell poles, future research could also investigate how these two proteins coordinate their activities, and where they lie within the hierarchy of proteins contributing to motility.

Our findings are the first to show that a CetZ family protein participates in multiple distinct roles. Taken together with the diversity and multiplicity of tubulin superfamily proteins in archaea[1, 15], it is likely that similar characteristics in early archaea led to the vast functional complexity, diversity, and specialisation of tubulins in eukaryotes. Our findings are also reminiscent of the fundamental roles of tubulin at the base of the eukaryotic flagellum, which originated before the last eukaryotic common ancestor[55-58]. Since flagellar basal body microtubules are derived from mitotic centrioles during eukaryotic cell differentiation, it is interesting to consider parallels to CetZ1 longitudinal filaments during rod formation[12, 13], followed by its polar localisation to promote stable assembly of the motility machinery in mature rod cells.

Acknowledgements

The authors would like to acknowledge S. Albers for providing strains and plasmids, as well as L. Cole and A. Bottomley from the UTS Microbial Imaging Facility. We acknowledge the use of the Cryo-Electron Microscopy Facility through the Victor Chang Cardiac Research Institute Innovation Centre, funded by the NSW government and the Electron Microscope Unit within the Mark Wainwright Analytical Centre (MWAC) at UNSW Sydney. The work was supported by the Australian Research Council (DP160101076 and FT160100010 to IGD).

Author contributions

Conceptualisation – HJB & IGD; Data curation – HJB, MII & JR; Formal analysis – HJB, MII & JR; Investigation – HJB, MII, JR; Methodology – all authors; Supervision – IGD, SI & MABB; Original draft – HJB; Revision – HJB & IGD; Reviewing the manuscript – all authors. Funding Acquisition – IGD.

References

1. Aylett CH, Duggin IG: **The tubulin superfamily in archaea**. In: *Prokaryotic Cytoskeletons.* Springer; 2017: 393-417.
2. Nogales E, Downing KH, Amos LA, Löwe J: **Tubulin and FtsZ form a distinct family of GTPases**. *Nature Structural and Molecular Biology* 1998, **5**(6):451.
3. Vaughan S, Wickstead B, Gull K, Addinall SG: **Molecular evolution of FtsZ protein sequences encoded within the genomes of archaea, bacteria, and eukaryota**. *Journal of molecular evolution* 2004, **58**(1):19-29.
4. Erickson HP: **Evolution of the cytoskeleton**. *Bioessays* 2007, **29**(7):668-677.
5. Erickson HP: **FtsZ, a prokaryotic homolog of tubulin?** *Cell* 1995, **80**(3):367-370.
6. Barton NR, Goldstein L: **Going mobile: microtubule motors and chromosome segregation**. *Proceedings of the National Academy of Sciences* 1996, **93**(5):1735-1742.
7. Appert-Rolland C, Ebbinghaus M, Santen L: **Intracellular transport driven by cytoskeletal motors: General mechanisms and defects**. *Physics Reports* 2015, **593**:1-59.
8. Hirokawa N, Noda Y, Tanaka Y, Niwa S: **Kinesin superfamily motor proteins and intracellular transport**. *Nature reviews Molecular cell biology* 2009, **10**(10):682-696.
9. An S, Deng Y, Tomsho JW, Kyoung M, Benkovic SJ: **Microtubule-assisted mechanism for functional metabolic macromolecular complex formation**. *Proceedings of the National Academy of Sciences* 2010, **107**(29):12872-12876.
10. Hawkins T, Mirigian M, Yasar MS, Ross JL: **Mechanics of microtubules**. *Journal of biomechanics* 2010, **43**(1):23-30.
11. Lutkenhaus J, Pichoff S, Du S: **Bacterial cytokinesis: from Z ring to divisome**. *Cytoskeleton* 2012, **69**(10):778-790.
12. Duggin IG, Aylett CH, Walsh JC, Michie KA, Wang Q, Turnbull L, Dawson EM, Harry EJ, Whitchurch CB, Amos LA: **CetZ tubulin-like proteins control archaeal cell shape**. *Nature* 2015, **519**(7543):362.
13. de Silva RT, Shinde V, Brown HJ, Liao Y, Duggin IG: **Dynamic self-association of archaeal tubulin-like protein CetZ1 drives Haloferax volcanii morphogenesis**. *bioRxiv* 2024:2024.2004. 2008.588506.
14. de Silva RT, Abdul-Halim MF, Pittrich DA, Brown HJ, Pohlschroder M, Duggin IG: **Improved growth and morphological plasticity of Haloferax volcanii**. *Microbiology* 2021.
15. Brown HJ, Duggin IG: **Diversity and Potential Multifunctionality of Archaeal CetZ Tubulin-like Cytoskeletal Proteins**. *Biomolecules* 2023, **13**(1):134.
16. Ithurbide S, de Silva RT, Brown HJ, Shinde V, Duggin IG: **A vector system for single and tandem expression of cloned genes and multi-colour fluorescent tagging in Haloferax volcanii**. *bioRxiv* 2024:2024.2003. 2013.584740.
17. Li Z, Kinosita Y, Rodriguez-Franco M, Nußbaum P, Braun F, Delpech F, Quax TE, Albers S-V: **Positioning of the motility machinery in halophilic archaea**. *MBio* 2019, **10**(3):e00377-00319.
18. Li Z, Rodriguez‐Franco M, Albers SV, Quax TE: **The switch complex ArlCDE connects the chemotaxis system and the archaellum**. *Molecular microbiology* 2020, **114**(3):468-479.
19. Quax TE, Altegoer F, Rossi F, Li Z, Rodriguez-Franco M, Kraus F, Bange G, Albers S-V: **Structure and function of the archaeal response regulator CheY**. *Proceedings of the National Academy of Sciences* 2018, **115**(6):E1259-E1268.
20. Albers S-V, Jarrell KF: **The archaellum: how Archaea swim**. *Frontiers in Microbiology* 2015, **6**:23.
21. Jarrell KF, Albers S-V: **The archaellum: an old motility structure with a new name**. *Trends in microbiology* 2012, **20**(7):307-312.
22. Jarrell KF, Albers S-V, Machado J: **A comprehensive history of motility and Archaellation in Archaea**. *FEMS Microbes* 2021, **2**.
23. Albers S-V, Jarrell KF: **The archaellum: an update on the unique archaeal motility structure**. *Trends in microbiology* 2018, **26**(4):351-362.
24. Beeby M, Ferreira JL, Tripp P, Albers S-V, Mitchell DR: **Propulsive nanomachines: the convergent evolution of archaella, flagella and cilia**. *FEMS microbiology reviews* 2020, **44**(3):253-304.
25. Briegel A, Oikonomou CM, Chang YW, Kjær A, Huang AN, Kim KW, Ghosal D, Nguyen HH, Kenny D, Ogorzalek Loo RR: **Morphology of the archaellar motor and associated cytoplasmic cone in Thermococcus kodakaraensis**. *EMBO reports* 2017, **18**(9):1660-1670.

26. Daum B, Vonck J, Bellack A, Chaudhury P, Reichelt R, Albers S-V, Rachel R, Kühlbrandt W: **Structure and in situ organisation of the Pyrococcus furiosus archaellum machinery**. *Elife* 2017, **6**:e27470.
27. Kupper J, Marwan W, Typke D, Grünberg H, Uwer U, Gluch M, Oesterhelt D: **The flagellar bundle of Halobacterium salinarium is inserted into a distinct polar cap structure**. *Journal of bacteriology* 1994, **176**(16):5184-5187.
28. Allers T, Barak S, Liddell S, Wardell K, Mevarech M: **Improved strains and plasmid vectors for conditional overexpression of His-tagged proteins in Haloferax volcanii**. *Applied and environmental microbiology* 2010, **76**(6):1759-1769.
29. Cline SW, Lam WL, Charlebois RL, Schalkwyk LC, Doolittle WF: **Transformation methods for halophilic archaebacteria**. *Canadian Journal of Microbiology* 1989, **35**(1):148-152.
30. Allers T, Ngo H-P, Mevarech M, Lloyd RG: **Development of additional selectable markers for the halophilic archaeon Haloferax volcanii based on the leuB and trpA genes**. *Applied and environmental microbiology* 2004, **70**(2):943-953.
31. Ducret A, Quardokus EM, Brun YV: **MicrobeJ, a tool for high throughput bacterial cell detection and quantitative analysis**. *Nature microbiology* 2016, **1**(7):1-7.
32. Schindelin J, Arganda-Carreras I, Frise E, Kaynig V, Longair M, Pietzsch T, Preibisch S, Rueden C, Saalfeld S, Schmid B: **Fiji: an open-source platform for biological-image analysis**. *Nature methods* 2012, **9**(7):676.
33. Tripepi M, Esquivel RN, Wirth R, Pohlschröder M: **Haloferax volcanii cells lacking the flagellin FlgA2 are hypermotile**. *Microbiology* 2013, **159**(Pt 11):2249.
34. Tripepi M, Imam S, Pohlschröder M: **Haloferax volcanii flagella are required for motility but are not involved in PibD-dependent surface adhesion**. *Journal of bacteriology* 2010, **192**(12):3093-3102.
35. Tripepi M, You J, Temel S, Önder Ö, Brisson D, Pohlschröder M: **N-glycosylation of Haloferax volcanii flagellins requires known Agl proteins and is essential for biosynthesis of stable flagella**. *Journal of bacteriology* 2012, **194**(18):4876-4887.
36. Abdul Halim MF, Pfeiffer F, Zou J, Frisch A, Haft D, Wu S, Tolić N, Brewer H, Payne SH, Paš a-Tolić L: **H aloferax volcanii archaeosortase is required for motility, mating, and C-terminal processing of the S-layer glycoprotein**. *Molecular microbiology* 2013, **88**(6):1164-1175.
37. Abdul Halim MF, Schulze S, DiLucido A, Pfeiffer F, Bisson Filho AW, Pohlschroder M: **Lipid Anchoring of Archaeosortase Substrates and Midcell Growth in Haloarchaea**. *mBio* 2020, **11**(2):e00349-00320.
38. Esquivel RN, Pohlschroder M: **A conserved type IV pilin signal peptide H-domain is critical for the post-translational regulation of flagella-dependent motility**. *Molecular microbiology* 2014, **93**(3):494-504.
39. Cerletti M, Martínez MJ, Giménez MI, Sastre DE, Paggi RA, De Castro RE: **The LonB protease controls membrane lipids composition and is essential for viability in the extremophilic haloarchaeon H aloferax volcanii**. *Environmental microbiology* 2014, **16**(6):1779-1792.
40. Chatterjee P, Garcia M, Cote J, Yun K, Legerme G, Habib R, Tripepi M, Young C, Kulp DW, Dyall-Smith M: **Involvement of ArlI, ArlJ, and CirA in Archaeal Type-IV Pilin-Mediated Motility Regulation**. *bioRxiv* 2024:2024.2003. 2004.583388.
41. Hackley RK, Hwang S, Herb JT, Bhanap P, Lam K, Vreugdenhil A, Darnell CL, Pastor MM, Martin JH, Maupin-Furlow JA: **TbsP and TrmB jointly regulate gapII to influence cell development phenotypes in the archaeon Haloferax volcanii**. *Molecular Microbiology* 2024.
42. Parente J, Casabuono A, Ferrari MC, Paggi RA, De Castro RE, Couto AS, Giménez MI: **A rhomboid protease gene deletion affects a novel oligosaccharide N-linked to the S-layer glycoprotein of Haloferax volcanii**. *Journal of Biological Chemistry* 2014, **289**(16):11304-11317.
43. Collins M, Afolayan S, Igiraneza AB, Schiller H, Krespan E, Beiting DP, Dyall-Smith M, Pfeiffer F, Pohlschroder M: **Mutations affecting HVO_1357 or HVO_2248 cause hypermotility in Haloferax volcanii, suggesting roles in motility regulation**. *Genes* 2021, **12**(1):58.
44. Nagel C, Machulla A, Zahn S, Soppa J: **Several one-domain zinc finger μ-proteins of Haloferax volcanii are important for stress adaptation, biofilm formation, and swarming**. *Genes* 2019, **10**(5):361.

45. Legerme G, Yang E, Esquivel RN, Kiljunen S, Savilahti H, Pohlschroder M: **Screening of a Haloferax volcanii transposon library reveals novel motility and adhesion mutants**. *Life* 2016, **6**(4):41.
46. Schiller H, Hong Y, Kouassi J, Rados T, Kwak J, DiLucido A, Safer D, Marchfelder A, Pfeiffer F, Bisson A: **Identification of structural and regulatory cell-shape determinants in Haloferax volcanii**. *Nature communications* 2024, **15**(1):1414.
47. Schiller H, Kouassi J, Hong Y, Rados T, Kwak J, DiLucido A, Safer D, Marchfelder A, Pfeiffer F, Bisson-Filho A: **Identification and characterization of structural and regulatory cell-shape determinants in Haloferax volcanii**. *bioRxiv* 2023:2023.2003. 2005.531186.
48. Schwarzer S, Rodriguez-Franco M, Oksanen HM, Quax TE: **Growth phase dependent cell shape of Haloarcula**. *Microorganisms* 2021, **9**(2):231.
49. Young KD: **The selective value of bacterial shape**. *Microbiology and molecular biology reviews* 2006, **70**(3):660-703.
50. Nußbaum P, Ithurbide S, Walsh JC, Patro M, Delpech F, Rodriguez-Franco M, Curmi PM, Duggin IG, Quax TE, Albers S-V: **An oscillating MinD protein determines the cellular positioning of the motility machinery in archaea**. *Current Biology* 2020, **30**(24):4956-4972. e4954.
51. Cerletti M, Giménez MI, Tröetschel C, D'Alessandro C, Poetsch A, De Castro RE, Paggi RA: **Proteomic Study of the Exponential–Stationary Growth Phase Transition in the Haloarchaea Natrialba magadii and Haloferax volcanii**. *Proteomics* 2018, **18**(14):1800116.
52. Prelich G: **Gene overexpression: uses, mechanisms, and interpretation**. *Genetics* 2012, **190**(3):841-854.
53. Mormile MR, Biesen MA, Gutierrez MC, Ventosa A, Pavlovich JB, Onstott TC, Fredrickson JK: **Isolation of Halobacterium salinarum retrieved directly from halite brine inclusions**. *Environmental Microbiology* 2003, **5**(11):1094-1102.
54. Schlesner M, Miller A, Besir H, Aivaliotis M, Streif J, Scheffer B, Siedler F, Oesterhelt D: **The protein interaction network of a taxis signal transduction system in a halophilic archaeon**. *BMC microbiology* 2012, **12**:1-20.
55. Carvalho-Santos Z, Azimzadeh J, Pereira-Leal JB, Bettencourt-Dias M: **Evolution: Tracing the origins of centrioles, cilia, and flagella**. *J Cell Biol* 2011, **194**(2):165-175.
56. Mitchell DR: **The evolution of eukaryotic cilia and flagella as motile and sensory organelles**. *Adv Exp Med Biol* 2007, **607**:130-140.
57. Moran J, McKean PG, Ginger ML: **Eukaryotic Flagella: Variations in Form, Function, and Composition during Evolution**. *BioScience* 2014, **64**(12):1103-1114.
58. Loreng TD, Smith EF: **The Central Apparatus of Cilia and Eukaryotic Flagella**. *Cold Spring Harb Perspect Biol* 2017, **9**(2).

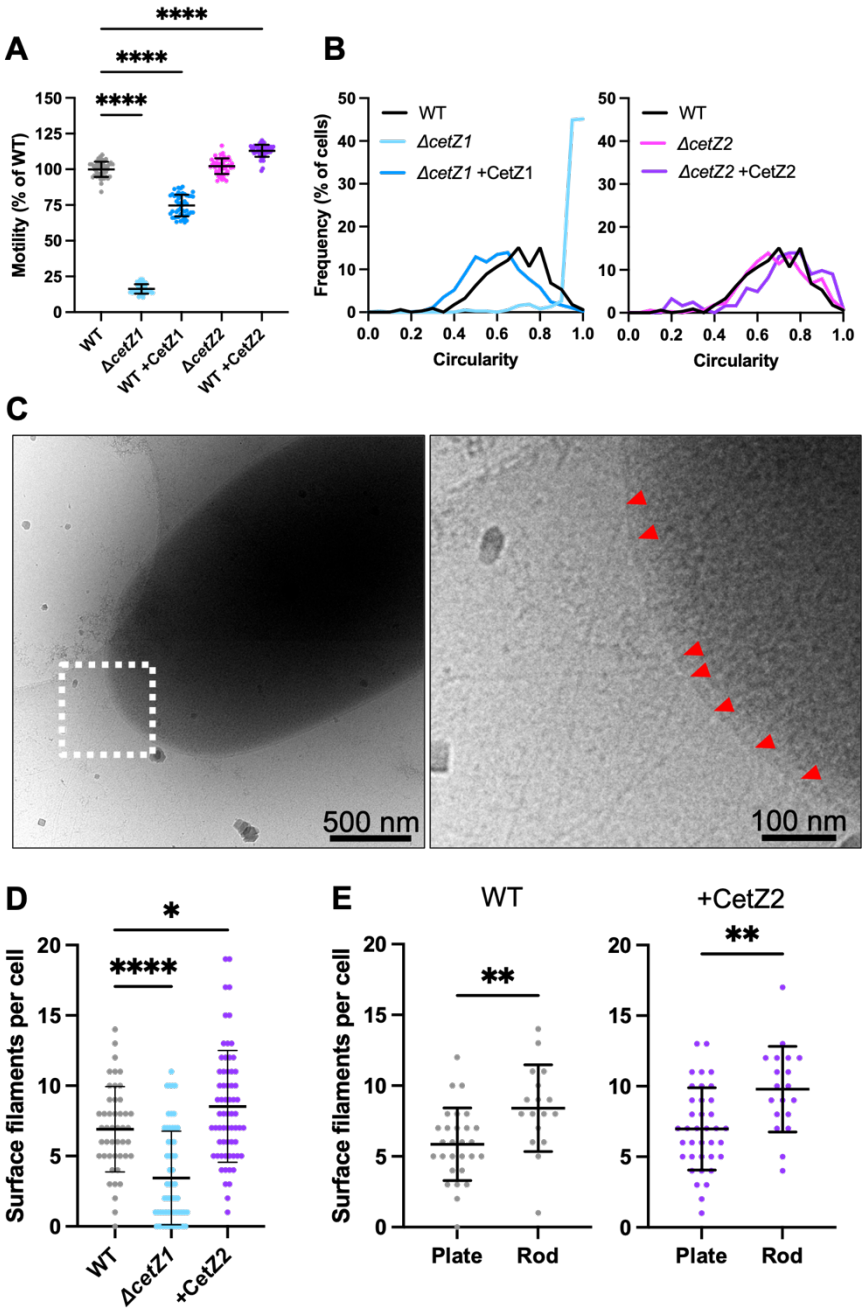

Figure 1. CetZs can contribute to motility without influencing shape. H26 wildtype, Δ*cetZ1* and Δ*cetZ2* strains with pTA962 vector only, and wildtype with *cetZ1* or *cetZ2* expressed from pTA962 as indicated (+CetZ1/2) were inoculated onto Hv-Cab soft-agar with 1 mM L-Tryptophan. **A)** Their motility halo diameters were quantified after four days and normalized to the mean of WT *H. volcanii* H26. Individual points represent biological replicates. **B)** . Circularity of individual cells extracted from the edge of motility halos was measured and is represented as a frequency distribution for wildtype and knockout *cetZ* strains with pTA962. CetZ1 and CetZ2 (+CetZ1/2) were expressed in their respective knockout backgrounds. Data for WT +pTA962 is displayed on both graphs for reference. The number of individual cells analysed for each strain is noted in Fig. S1. **C)** Representative CryoEM image of H26 wildtype cells (left) and zoom (right) showing surface filaments (red tick marks). **D)** The number of surface filaments per cell were manually counted using images obtained in **C** for H26 wildtype, Δ*cetZ1*, and +CetZ2 strains. The number of cells analysed per strain is as follows: WT +pTA962, n=46; Δ*cetZ1* +pTA962, n=58; WT +CetZ2, n=66. **E)** For rod forming strains, WT and +CetZ2, the number of surface filaments per cell was determined for rod and plate-shaped cells. Data in **D** and **E** was obtained from the same samples. **A, D,** and **E** show mean and standard deviation. **A** and **D** use one-way ANOVA as a statistical test, and **E** uses an un-paired T-test. ****p<0.00005, **p<0.005, *p<0.05.

686

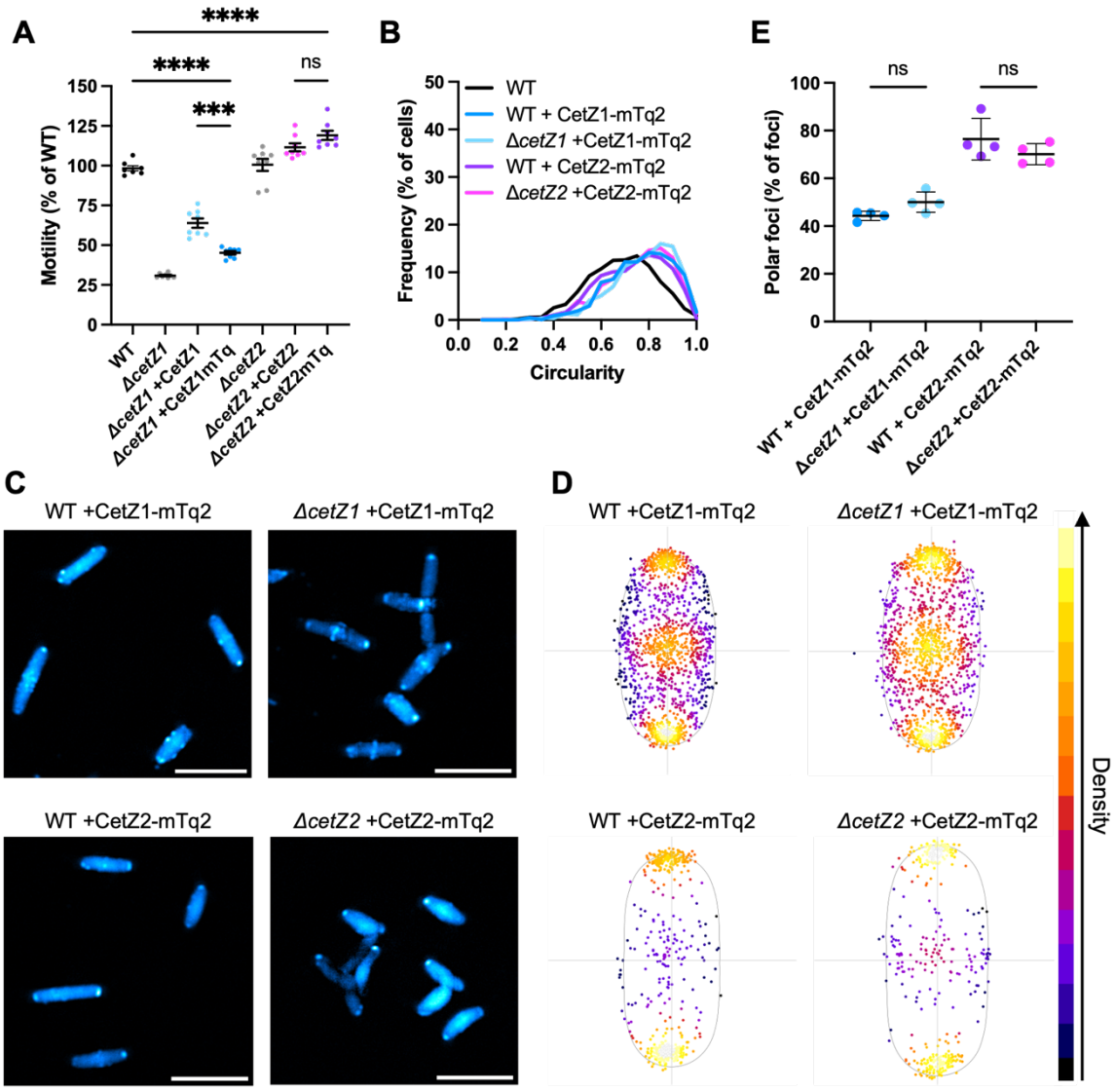

687

688

689 **Figure 2. Localisation of CetZ1 and CetZ2 in motile cells.** CetZ1-mTq2 and CetZ2-mTq2 fusion proteins
690 were expressed in H26 wildtype cells and their respective knockout backgrounds. H26 wildtype, Δ*cetZ1,*
691 and Δ*cetZ2* with pTA962, and Δ*cetZ1* +CetZ1, and Δ*cetZ2* + CetZ2 were used as controls. **A)** Strains were
692 inoculated onto Hv-Cab soft-agar with 1 mM L-Tryptophan and their motility halo diameters were quantified.
693 Individual points represent biological replicates. **(B)** Cells expressing CetZ1 or CetZ2-mTq2 fusions were
694 extracted from the edge of the motility halo and their circularity was measured using phase-contrast
695 microscopy images (not shown). **C)** Fluorescence microscopy was also conducted to observe CetZ1 and
696 CetZ2 localisation in these cells. **D)** Heatmap representations of CetZ1 and CetZ2 localisation in motile
697 cells. **E)** Proportion of detected CetZ foci located at cell poles. In **A** and **E**, mean and standard deviation are
698 shown. One-way ANOVA was used as a statistical test, and only significant and/or relevant comparisons
699 are shown on graphs. ****p<0.00005, ***p<0.0005, ns=not significant. The number of cells analysed for
700 each strain in **B-E** was as follows: WT +pTA962, n=2046; WT +CetZ1-mTq2, n=1193; Δ*cetZ1* +CetZ1-mTq2,
701 n=1672; WT +CetZ2-mTq2, n=1338; Δ*cetZ2* +CetZ2-mTq2, n=861.

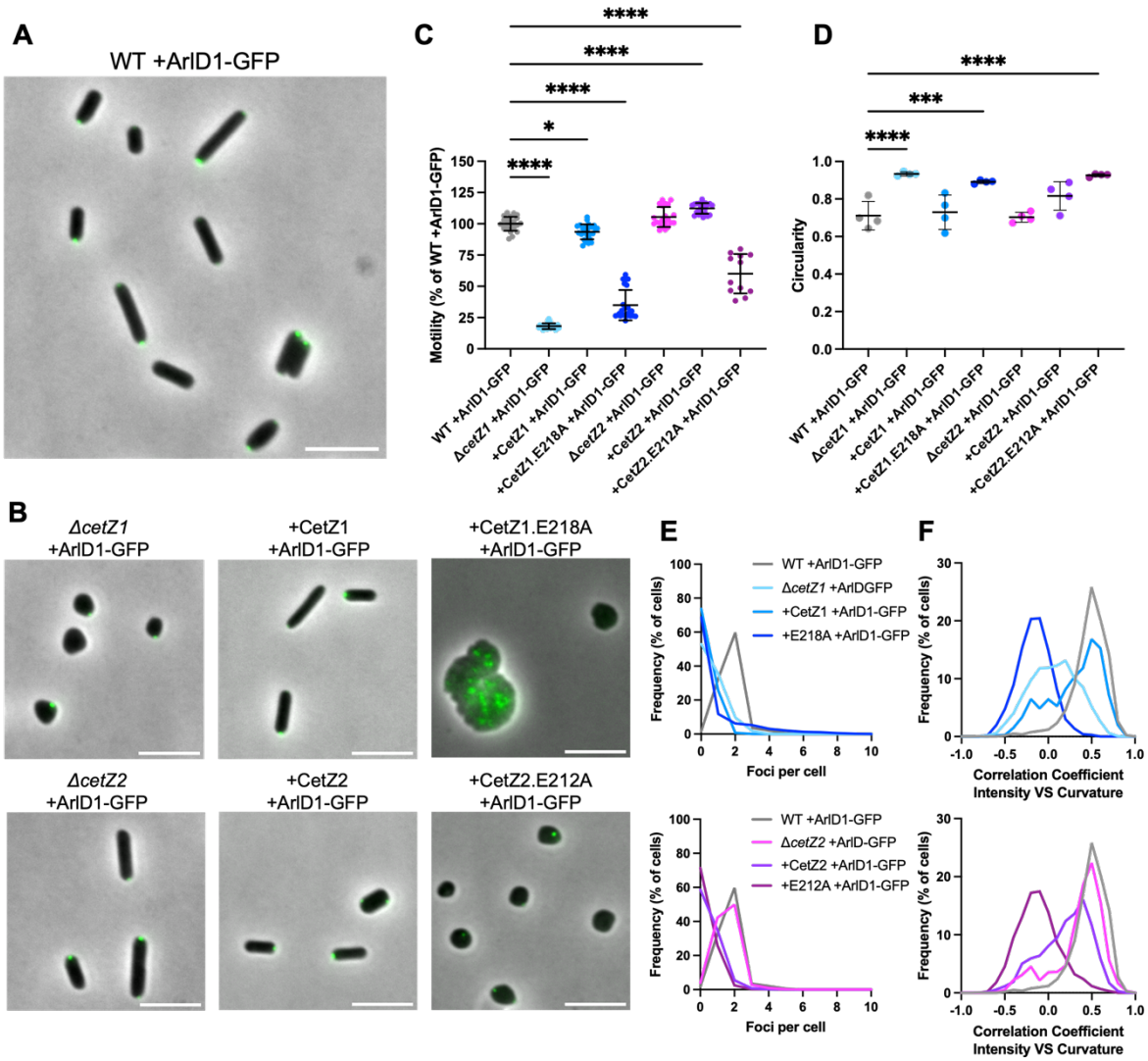

Figure 3. ArlD1 localisation in CetZ mutant strains. ArlD1-GFP was expressed from pSVA3919 in H26 wildtype, Δ*cetZ1*, and Δ*cetZ2*, or was co-expressed with CetZ1, CetZ1.E218A, CetZ2, or CetZ2.E212A from pHJB31, pHJB34, pHJB37, or pHJB40, respectively, in H26 wildtype. These strains were inoculated onto Hv-Cab soft-agar with 1 mM L-Tryptophan and extracted from the halo-edge for **A-B)** phase-contrast and fluorescence microscopy. Four biological replicates were carried out for each strain. Scale bar: 5 µm. **C)** Motility halo diameters for each strain were quantified. Individual points represent biological replicates. **D)** Phase-contrast images were used to measure circularity. Individual points represent the mean of all cell circularities in a biological replicate. In **C** and **D** mean and standard deviation are shown. One-way ANOVA was used as a statistical test. ****p<0.00005, ***p<0.0005, **p<0.005, *p<0.05. Only significant comparisons are shown. **E)** Frequency distributions of the number of foci per cell in each strain, and **F)** the Pearson Correlation Coefficient between local membrane curvature and fluorescence intensity. In **E** and **F**, data for WT +ArlD1-GFP is displayed on all graphs for reference, and the key refers to both panels. For **D-F** the number of cells pooled from four biological replicates for each strain is as follows: WT +ArlD1-GFP, n=2240; Δ*cetZ1* +ArlD1-GFP, n=1097; WT +CetZ1 +ArlD1-GFP, n=1448; WT +CetZ1.E218A +ArlD1-GFP, n=2007; Δ*cetZ2* +ArlD1-GFP, n=1249; WT +CetZ2 +ArlD1-GFP, n=1655; WT +CetZ2.E212A +ArlD1-GFP, n=1466.

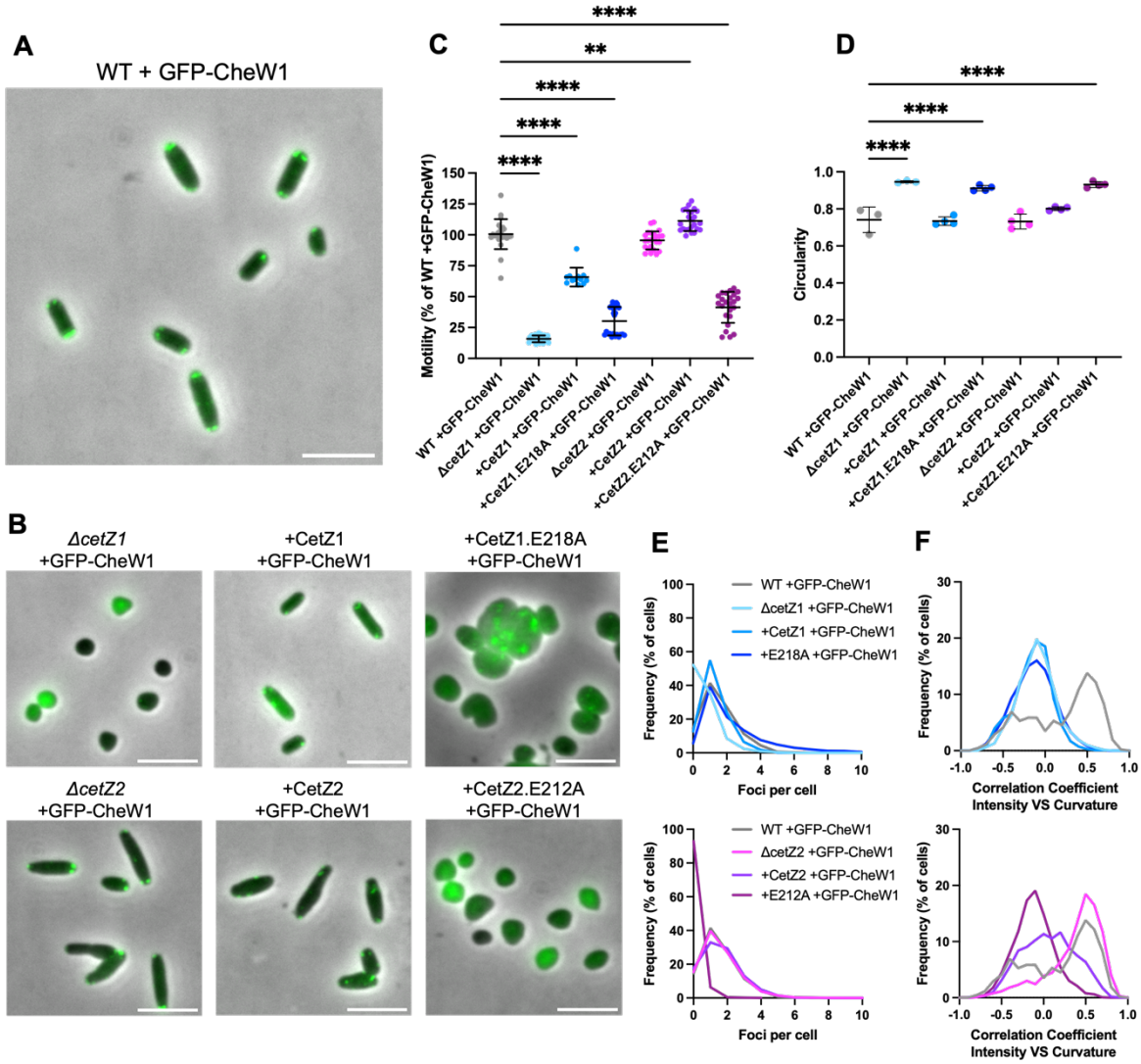

Figure 4. CheW1 localisation in CetZ mutant strains. GFP-CheW1 was expressed from pSVA5031 in H26 wildtype, Δ*cetZ1*, and Δ*cetZ2*, or was co-expressed with CetZ1, CetZ1.E218A, CetZ2, or CetZ2.E212A from pHJB32, pHJB35, pHJB38, or pHJB41, respectively, in H26 wildtype. These strains were inoculated onto Hv-Cab soft-agar with 1 mM L-Tryptophan and extracted from the halo-edge. **A-F** is as described in Figure 3. For **D-F** the number of cells pooled from four biological replicates for each strain is as follows: WT +GFP-CheW1, n=1792; Δ*cetZ1* +GFP-CheW1, n=2458; WT +CetZ1 +GFP-CheW1, n=2195; WT +CetZ1.E218A +GFP-CheW1, n=3834; Δ*cetZ2* +GFP-CheW1, n=3222; WT +CetZ2 +GFP-CheW1, n=2121; WT +CetZ2.E212A +GFP-CheW1, n=4055.

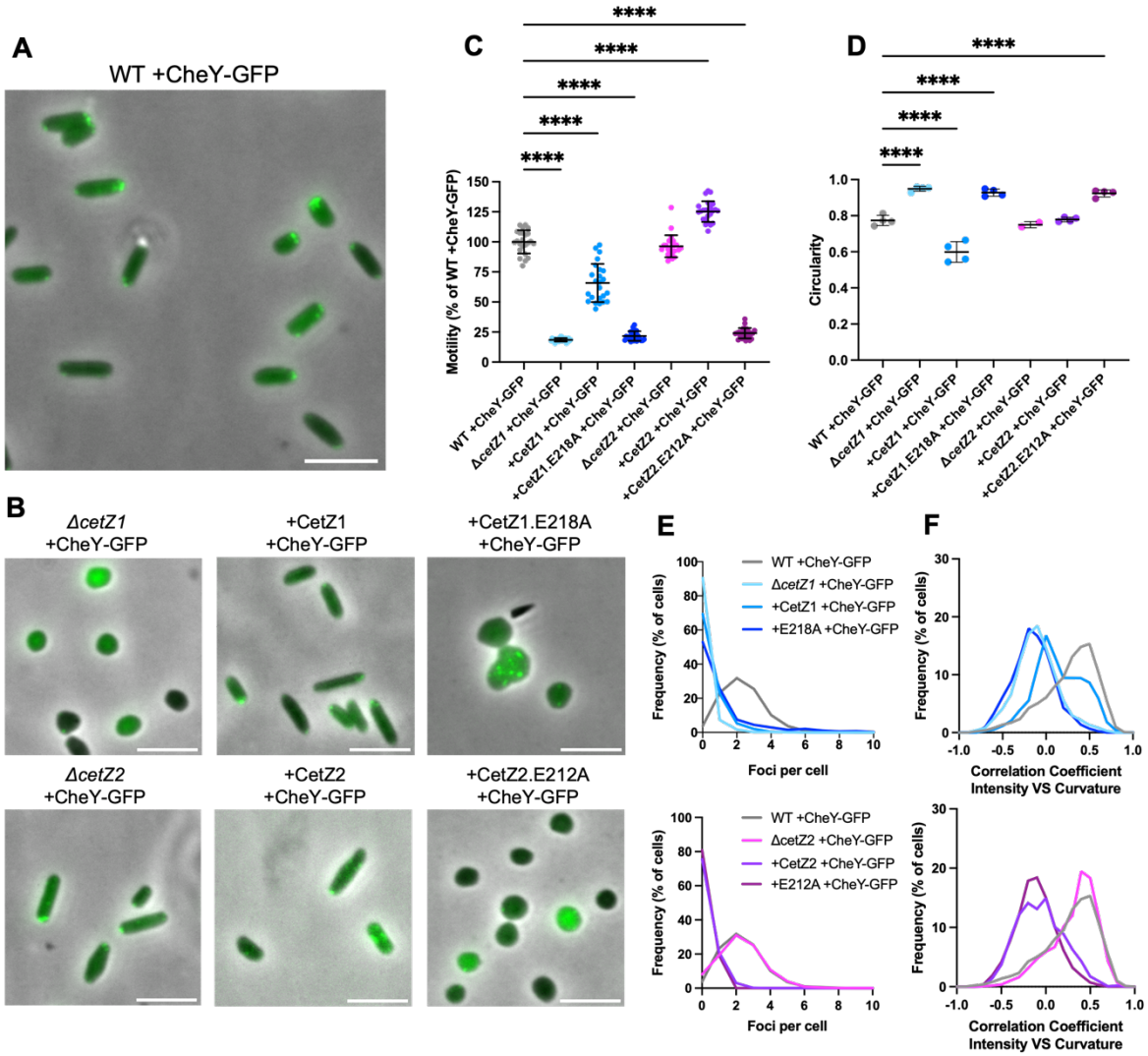

Figure 5. CheY localisation in CetZ mutant strains. CheY-GFP was expressed from pSVA5611 in H26 wildtype, Δ*cetZ1*, and Δ*cetZ2*, or was co-expressed with CetZ1, CetZ1.E218A, CetZ2, or CetZ2.E212A from pHJB33, pHJB36, pHJB39, or pHJB42, respectively, in H26 wildtype. These strains were inoculated onto Hv-Cab soft-agar with 1 mM L-Tryptophan and extracted from the halo-edge. **A-F** is as described in Figure 3. For **D-F** the number of cells pooled from four biological replicates for each strain is as follows: WT +CheY-GFP, n=2892; Δ*cetZ1* +CheY-GFP, n=1825; WT +CetZ1 +CheY-GFP, n=1490; WT +CetZ1.E218A +CheY-GFP, n=1704; Δ*cetZ2* +CheY-GFP, n=1341; WT +CetZ2 +CheY-GFP, n=1833; WT +CetZ2.E212A +CheY-GFP, n=2422.